Self-consistent Hartree description of deformed nuclei in a relativistic quantum field theory

C. E. Price* and G. E. Walker
Physics Department and Nuclear Theory Center, Indiana University, Bloomington, Indiana 47405
(Received 24 November 1986)

Relativistic Hartree orbitals for nonspherical (even-even) nuclei have been calculated self-consistently from a Lagrangian field theory using the mean field approximation. All parameters in this model are determined from the properties of infinite nuclear matter, so there are no parameters which can be adjusted in the calculation of the orbitals. The energy levels, rms radii, and quadrupole moments are in qualitative agreement with earlier nonrelativistic calculations and with experiment; however, the overall deformations (which are fixed by the self-consistency) are somewhat smaller than those obtained experimentally and from nonrelativistic calculations. The difference may be due to the large compressibility characteristic of relativistic mean field calculations. These orbitals and the self-consistently determined mean fields provide a framework for a detailed investigation of the compressibility as well as other relativistic effects.

I. INTRODUCTION

In the past few years there has been considerable interest in the role of the Dirac equation in nuclear physics, both in scattering processes,[1] and in nuclear structure.[2] This interest has been encouraged by the promising results of Dirac phenomenology[3] and by the development of a consistent relativistic mean-field theory.[4]

Using the Dirac equation with phenomenological Lorentz scalar and vector potentials, it is possible to obtain good fits to both the cross section and analyzing power for a wide range of intermediate energy nucleon-nucleus elastic scattering processes. Furthermore, having determined the free parameters of the potentials from these fits, it is possible to predict the correct angular dependence of the spin rotation parameter,[5] Q. Traditional nonrelativistic calculations were unable to achieve these results at energies above approximately 400 MeV, particularly with respect to the spin observables.

Another indication of the potential importance of relativity in nuclear physics comes from the development of quantum hadrodynamics[6] (QHD) and the relativistic Hartree approximation for nuclear structure. The basis of QHD is a renormalizable quantum field theory Lagrangian which explicitly contains Lorentz scalar and four-vector meson fields. In the high density limit of infinite nuclear matter, the quantum meson fields may be replaced by their expectation values which are classical fields. In fact, the mean field approximation has been utilized at normal nuclear densities. In this case the unknown coupling constants and masses of these mean meson fields are adjusted to reproduce the correct binding energy and saturation density of nuclear matter. In agreement with the results of Dirac phenomenology, it is found that this procedure leads to very large (roughly 400 MeV) attractive scalar and repulsive vector fields whose net contribution to the potential is comparable to nonrelativistic models. This makes it possible to see large relativistic effects arising from situations in which these fields do not cancel. Such a situation is seen when this model is extended to calculations for finite nuclei. By allowing a radial spatial dependence in the mean fields, a self-consistent relativistic shell model can be developed for spherical nuclei using the Hartree approximation.[7] In these calculations it is found that the simple scalar and vector fields are sufficient to give the correct spin-orbit splittings of the energy levels. This is possible because the spin-orbit force arises from the sum of the scalar and vector fields rather than their difference. QHD and the relativistic Hartree approximation provide a well-defined method for obtaining relativistic spherical shell model orbitals, which include much of the important physics.

The results of this work have been applied to calculations of nuclear magnetic moments,[8,9] relativistic nuclear structure (RPA),[2,10] muon capture, beta decay and electron scattering form factors,[11] and the electric dipole sum rule;[12] the results are encouraging. However, the validity of the mean field approximation and of the appropriateness of the Lagrangians used in the simple relativistic theories to date are largely untested. Corrections to the mean field approximation due to the inclusion of Fock terms or vacuum polarization effects can be appreciable (~ 10–20%).[6] Moreover, a successful theory involving pions (in the limit where their contribution is nonvanishing) does not yet exist. Because of these uncertainties it is useful to test the existing models in other domains. For these reasons, we have developed a calculational procedure for making predictions for a certain class of deformed nuclei in a relativistic model. It is important to stress that the reason for pursuing this work was not that there exists some deficiency in previous nonrelativistic structure calculations in deformed nuclei which this calculation is expected to rectify. The early work on deformed nuclei[13,14] was on the same general level as the current calculation. It involved Hartree-Fock calculations in a limited basis, and, in general, gave reasonable results for many of the nuclei considered. The major advantage of the present calculation is that the interaction is derived self-consistently from a relativistic nuclear field theory in which the parameters are determined from the bulk prop-

erties of nuclear matter. When applied to the deformed system there are no adjustable parameters and the equilibrium deformation is determined through the self-consistency of the solution.

Modern nonrelativistic structure calculations are much more sophisticated than the present model, for example, utilizing Hartree-Fock Bogoliubov techniques[15] or the interacting boson model.[16] It is not expected that the present work could replace these calculations, but it hopefully represents a first step toward sophisticated, self-consistent, relativistic calculations in deformed nuclei as well as testing the present relativistic approach in a new domain.

II. FORMALISM

As in the work of Serot and Horowitz, we chose as our starting point a quantum field theory Lagrangian which includes the coupling of the nucleons (ψ) to sigma (ϕ), omega (V), pi (π), and rho (b) mesons and the photon (A):[7,17]

$$\begin{aligned} L = {} & \bar{\psi}(i\partial\!\!\!/ - M)\psi + \tfrac{1}{2}(\partial_\mu\phi\partial^\mu\phi - m_s^2\phi^2) - \tfrac{1}{4}G_{\mu\nu}G^{\mu\nu} + \tfrac{1}{2}m_v^2 V_\mu V^\mu \\ & + g_s\bar{\psi}\psi\phi - g_v\bar{\psi}\gamma_\mu\psi V^\mu + \tfrac{1}{2}(\partial_\mu\boldsymbol{\pi}\cdot\partial^\mu\boldsymbol{\pi} - m_\pi^2\boldsymbol{\pi}\cdot\boldsymbol{\pi}) - ig_\pi\bar{\psi}\gamma_5\boldsymbol{\tau}\cdot\boldsymbol{\pi}\psi - \tfrac{1}{4}\mathbf{B}_{\mu\nu}\cdot\mathbf{B}^{\mu\nu} + \tfrac{1}{2}m_\rho^2\mathbf{b}_\mu\cdot\mathbf{b}^\mu - \tfrac{1}{2}g_\rho\bar{\psi}\gamma_\mu\boldsymbol{\tau}\cdot\mathbf{b}^\mu\psi - \tfrac{1}{4}F_{\mu\nu}F^{\mu\nu} \\ & - eA_\mu(\bar{\psi}\gamma^\mu\tfrac{1}{2}(1+\tau_3)\psi + (\mathbf{b}_\nu\times\mathbf{B}^{\nu\mu})_3 + \{\boldsymbol{\pi}\times[\partial^\mu\boldsymbol{\pi} + g_\rho(\boldsymbol{\pi}\times\mathbf{b}^\mu)]\}_3) , \end{aligned} \tag{1}$$

where

$$\begin{aligned} F_{\mu\nu} &\equiv \partial_\mu A_\nu - \partial_\nu A_\mu , \\ G_{\mu\nu} &\equiv \partial_\mu V_\nu - \partial_\nu V_\mu , \\ B_{\mu\nu} &\equiv \partial_\mu b_\nu - \partial_\nu b_\mu - g_\rho(\mathbf{b}_\mu\times\mathbf{b}_\nu) . \end{aligned} \tag{2}$$

The particular form of the pion couplings given in Eq. (1) and the fact that a relativistic theory satisfactorily incorporating pions has still not been developed is not central to our discussion, because as will be discussed below, the pion contributions vanish in the mean field approximation. Thus for our purposes, pion terms could be simply dropped from the model Lagrangian equation (1). From this Lagrangian, using the mean field approximation for the meson fields and following the techniques discussed in Ref. 7, we can derive the following general equations of motion:

$$(\nabla^2 - m_s^2)\phi(\mathbf{x}) = -g_s\mathrm{Tr}[iG_H(\mathbf{x},\mathbf{x})] , \tag{3}$$

$$(\nabla^2 - m_v^2)V^\mu(\mathbf{x}) = -g_v\mathrm{Tr}[i\gamma^\mu G_H(\mathbf{x},\mathbf{x})] , \tag{4}$$

$$(\nabla^2 - m_\pi^2)\pi^a(\mathbf{x}) = -g_\pi\mathrm{Tr}[i\gamma_5\tau^a G_H(\mathbf{x},\mathbf{x})] , \tag{5}$$

$$(\nabla^2 - m_\rho^2)b^{\mu a}(\mathbf{x}) = -\tfrac{1}{2}g_\rho\mathrm{Tr}[i\gamma^\mu\tau^a G_H(\mathbf{x},\mathbf{x})] , \tag{6}$$

$$\nabla^2 A^\mu(\mathbf{x}) = -e\,\mathrm{Tr}[i\gamma^\mu\tfrac{1}{2}(1+\tau^3)G_H(\mathbf{x},\mathbf{x})] , \tag{7}$$

$$[-i\boldsymbol{\alpha}\cdot\boldsymbol{\nabla} + \gamma_0 M + \gamma_0\Sigma_H(\mathbf{x})]U_\alpha(\mathbf{x}) = \epsilon_\alpha U_\alpha(\mathbf{x}) , \tag{8}$$

where U_α is a nucleon orbital with quantum numbers α,

$$\begin{aligned} \Sigma_H(\mathbf{x}) = {} & -g_s\phi(\mathbf{x}) + g_v\gamma_\mu V^\mu(\mathbf{x}) + g_\pi\gamma_5\tau_a\pi^a(\mathbf{x}) \\ & + \tfrac{1}{2}g_\rho\gamma_\mu\tau_a b^{\mu a}(\mathbf{x}) + \tfrac{1}{2}e\gamma_\mu(1+\tau_3)A^\mu(\mathbf{x}) \end{aligned} \tag{9}$$

is the Hartree self-energy, and

$$\begin{aligned} iG_H(\mathbf{x},\mathbf{y}) = \sum_\alpha U_\alpha(\mathbf{x})\bar{U}_\alpha(\mathbf{y})[\,& \theta(x^0-y^0)\theta(\epsilon_\alpha-\epsilon_F) \\ & - \theta(y^0-x^0)\theta(\epsilon_F-\epsilon_\alpha)] \end{aligned} \tag{10}$$

is the Hartree propagator (ϵ_F is the energy of the highest filled level). For the purposes of this calculation we have chosen to limit the type of deformation considered to azimuthally and reflection symmetric systems (i.e., prolate and oblate ellipsoids for the lowest order deformation). This limitation effectively limits the calculation to even-even nuclei in which states with $j_z = \pm m$ are degenerate. The advantage of this limitation is that for this symmetry many of the traces in Eqs. (3)–(7) vanish. It is simple to show that the traces in Eqs. (4), (6), and (7) vanish if $\mu \neq 0$; this eliminates all of the three vector components of the boson fields. Also, the isospin traces in Eqs. (5) and (6) vanish if $a \neq 0$; this eliminates all of the charged mesons (π^0 and ρ^0 remain). Finally, the remaining trace in Eq. (5) vanishes due to the presence of the γ_5; this eliminates the contribution of the pion in the Hartree approximation for a nucleus possessing good parity. So, the limitation on the type of deformation to be considered greatly simplifies the calculation by limiting the contributing bosons to the scalar meson, the zero components of the isoscalar vector meson and the photon, and the zero component of the neutral rho meson. This is the same set of bosons that was required for spherical nuclei; however, these boson fields now have an additional angular dependence.

In principle, we could solve these equations with no further approximation; however, due to the difficulties often encountered in solving coupled partial differential equations, it is useful to expand the angular dependence of the mean fields in some convenient basis. Therefore, the boson fields are expanded in terms of Legendre polynomials

$$\phi(r,\theta) = \sum_l \phi_l(r)P_l(\cos\theta) , \tag{11}$$

where from symmetry considerations, only even values of l are required; and the nucleon orbitals are expanded in terms of spherical spin angle functions[20]

$$U_\alpha(x)=U_{nmt}=\sum_{\kappa'}\begin{bmatrix}\dfrac{iG_{n\kappa' t}(r)}{r}\Phi_{\kappa' m}\\ \dfrac{-F_{n\kappa' t}(r)}{r}\Phi_{-\kappa' m}\end{bmatrix}\eta_t\ , \tag{12}$$

where, again, the symmetry limits the required values of κ'. As is clear from Eq. (12), the total angular momentum, j, of the individual orbitals is no longer a good quantum number. This is a general result for deformed systems and will lead to additional difficulties which will be discussed below.

Using these expansions the equations of motion have the following form:

$$(\nabla_s^2-m_s^2)\phi(r,\theta)=-g_s\rho_s(r,\theta)=-g_s\sum_l\left[\frac{2l+1}{4\pi r^2}\right]P_l(\cos\theta)\sum_{\alpha\kappa\kappa'}^{\text{occ}}[G_{\alpha\kappa}(r)G_{\alpha\kappa'}(r)-F_{\alpha\kappa}(r)F_{\alpha\kappa'}(r)]A(l,\kappa',\kappa,m)\ , \tag{13}$$

$$(\nabla^2-m_v^2)V^0(r,\theta)=-g_v\rho_{\rm B}(r,\theta)=-g_v\sum_l\left[\frac{2l+1}{4\pi r^2}\right]P_l(\cos\theta)\sum_{\alpha\kappa\kappa'}^{\text{occ}}[G_{\alpha\kappa}(r)G_{\alpha\kappa'}(r)+F_{\alpha\kappa}(r)F_{\alpha\kappa'}(r)]A(l,\kappa',\kappa,m)\ , \tag{14}$$

$$(\nabla^2-m_\rho^2)b^0(r,\theta)=-\tfrac{1}{2}g_\rho\rho_3(r,)=-\tfrac{1}{2}g_\rho\sum_l\left[\frac{2l+1}{4\pi r^2}\right]P_l(\cos\theta)\sum_{\alpha\kappa\kappa'}^{\text{occ}}(-)^{t_\alpha-(1/2)}[G_{\alpha\kappa}(r)G_{\alpha\kappa'}(r)+F_{\alpha\kappa}(r)F_{\alpha\kappa'}(r)]A(l,\kappa',\kappa,m)\ , \tag{15}$$

$$\nabla^2A^0(r,\theta)=-e\rho_p(r)=-e\sum_l\left[\frac{2l+1}{4\pi r^2}\right]P_l(\cos\theta)\sum_{\alpha\kappa\kappa'}^{\text{occ}}(t_\alpha+\tfrac{1}{2})[G_{\alpha\kappa}(r)G_{\alpha\kappa'}(r)+F_{\alpha\kappa}(r)F_{\alpha\kappa'}(r)]A(l,\kappa',\kappa,m)\ , \tag{16}$$

$$\frac{d}{dr}G_{\alpha\kappa}(r)+\frac{\kappa}{r}G_{\alpha\kappa}(r)-(\epsilon_\alpha+M)F_{\alpha\kappa}(r)+\sum_{l,\kappa'}[g_s\phi_l(r)+g_vV_l^0(r)+t_\alpha g_\rho b_l^0(r)+(t_\alpha+\tfrac{1}{2})eA_l^0(r)]A(l,\kappa',\kappa,m)F_{\alpha\kappa'}(r)=0\ , \tag{17}$$

$$\frac{d}{dr}F_{\alpha\kappa}(r)-\frac{\kappa}{r}F_{\alpha\kappa}(r)+(\epsilon_\alpha-M)G_{\alpha\kappa}(r)+\sum_{l,\kappa'}[g_s\phi_l(r)-g_vV_l^0(r)-t_\alpha g_\rho b_l^0(r)-(t_\alpha+\tfrac{1}{2})eA_l^0(r)]A(l,\kappa',\kappa,m)G_{\alpha\kappa'}(r)=0\ , \tag{18}$$

where

$$A(l,\kappa',\kappa,m)=(-)^{(1/2)+m}[(2j_\kappa+1)(2j_{\kappa'}+1)]^{1/2}\begin{pmatrix}j_{\kappa'} & l & j_\kappa\\ -m & 0 & m\end{pmatrix}\begin{pmatrix}j_{\kappa'} & l & j_\kappa\\ \frac{1}{2} & 0 & -\frac{1}{2}\end{pmatrix}, \tag{19}$$

and $\rho_{\rm B}$ and ρ_s represent the baryon and scalar densities, respectively. This set of equations, although somewhat complicated, may be solved numerically in a straightforward manner. (The details of the numerical methods are outlined in the Appendix.) The value of using the expansions given above is clear from the form of Eqs. (13)–(19) which are now simply coupled ordinary differential equations rather than coupled partial differential equations. These equations contain all information about the static ground state including the equilibrium deformation.

The six parameters in Eqs. (13)–(18) must be determined before proceeding with the solution of a deformed system. The ratios of the coupling constants and the corresponding meson masses are determined in the limit of infinite nuclear matter by requiring that the model reproduce the correct saturation density (corresponding to $k_F=1.3$ fm^{-1}), bulk binding energy (15.75 MeV/nucleon) and bulk symmetry energy (35 MeV/nucleon). The vector and rho couplings are then fixed by taking the corresponding masses from the empirically observed ω and ρ mesons. Since there is no low-lying scalar meson, the scalar mass (at constant g_s^2/m_s^2) is adjusted to reproduce the charge radius of ^{40}Ca in a finite nucleus calculation using the spherical limit of Eqs. (13)–(19). For more detail on the determination of the parameters and on QHD in general see Ref. 6.

III. ANGULAR MOMENTUM PROJECTION

As mentioned above the single particle states obtained by solving the Hartree equations of motion in the deformed system do not have good total angular momentum (although the z projection is still a good quantum number for the assumed symmetry), so it is not expected that a simple product wave function for the ground state will have good total angular momentum, J. For this reason, the Hartree ground state obtained as outlined above and in the Appendix is only an intrinsic state which must still be related to the actual ground state. For even-even nuclei the ground state should have $J=0$ and in order to obtain such a state from the product wave function it is necessary to project out a state with good total angular momentum.[21,22] This is generally done by the projection method of Peierls and Yoccoz.[23] The Hartree intrinsic wave function actually represents a class of many particle wave functions, $\Phi(\mathbf{r};\omega)$, that are distinguished by the parameter ω which designates the orientation in space of the axis of symmetry. Clearly, wave functions that differ only

by such an orientation are degenerate and must be superposed in the correct linear combination in order to form a proper ground state. This class of wave functions may be represented as

$$\Phi_K(\mathbf{r};\omega)=R(\omega)\Phi_K(\mathbf{r}) , \tag{20}$$

where K is the third component of angular momentum of the intrinsic state, $\Phi_K(\mathbf{r})$, and $R(\omega)$ is the rotation operator[19]

$$R(\omega)=e^{-i\alpha J_z}e^{-i\beta J_y}e^{-i\gamma J_x} . \tag{21}$$

In Eq. (21) α, β, and γ are the usual Euler angles corresponding to the orientation ω. With this representation the Peierls Yoccoz wave function is

$$\Psi_{JKM}(\mathbf{r})=\int d\omega D^J_{MK}(\omega)\Phi_K(\mathbf{r};\omega) , \tag{22}$$

where J and M represent the total angular momentum and its z component for the projected state Ψ_{JKM}. For the present calculation $K=0$ since we have filled the $\pm m$ states in pairs, and $J=M=0$ since we are interested in the ground state.

In practice, there are a variety of techniques for performing the integrals necessary for a correct treatment of the angular momentum projection; however, for the remainder of this paper we will restrict the discussion to intrinsic state properties or quantities which may be extracted from the intrinsic state by some reasonable approximation without performing the full angular momentum projection.

IV. RESULTS

Using the Hartree equations and the solution methods discussed in the Appendix we have solved for the intrinsic states of the following nuclei: ^{12}C, ^{16}O, ^{20}Ne, ^{24}Mg, ^{40}Ca, ^{42}Ca, ^{44}Ca, and ^{48}Ca. The two closed-shell nuclei, ^{16}O and ^{40}Ca, are expected to be spherical and the importance of their solutions is discussed in the Appendix. For the remaining nuclei which are expected to have an equilibrium deformation we must specify the level ordering which is to be used in the calculation. This level ordering determines the orbitals that will be filled in the solution even though they may not be the orbitals that lead to the lowest energy ground state. For this reason the level ordering must be carefully chosen and the effects of using different level orderings must be investigated. In practice, we have used several criteria for selecting the level ordering. First, since strongly bound orbitals are expected to be only slightly affected by the deformation, we used the usual spherical well level ordering for orbitals whose energies are not near the energy surface. Second, for levels which are relatively loosely bound we used as a guide both previous nonrelativistic calculations[13,14] and nonrelativistic Nilsson diagrams.[24] It is not possible for us to calculate a relativistic equivalent of the Nilsson diagram because the deformation is determined through the self-consistency of the solution, and any solution found by artificially enforcing a specific deformation need not be related to the actual solution. For the nuclei presented here, we have also used trial and error to vary the level ordering and compare the binding energies of the solutions. Thus far the level orderings found in this manner are in agreement with the nonrelativistic work.

TABLE I. Two alternative level orderings in ^{20}Ne.

Prolate		Oblate	
Level	Energy	Level	Energy
$\frac{1}{2}^+$	−45.6	$\frac{1}{2}^+$	−46.4
$\frac{1}{2}^-$	−28.6	$\frac{3}{2}^-$	−27.0
$\frac{3}{2}^-$	−22.9	$\frac{1}{2}^-$	−25.4
$\frac{1}{2}^-$	−15.6	$\frac{1}{2}^-$	−17.1
$\frac{1}{2}^+$	−12.1	$\frac{1}{2}^+$	−9.4
$\frac{3}{2}^+$	−8.1	$\frac{3}{2}^+$	−7.8
$Q=403$ mb		$Q=-199$ mb	
$E_0=-103.3$ MeV		$E_0=-98.5$ MeV	

In Table I, we show the neutron energy levels for ^{20}Ne assuming two slightly different level orderings. The general trend of the level energies is very similar, except for the order of the lowest $\frac{1}{2}^-$ and $\frac{3}{2}^-$ states. As expected the $\frac{3}{2}^-$ is more tightly bound in the oblate solution and the $\frac{1}{2}^-$ is more tightly bound in the prolate solution. In both solutions, the energy gap between the bound and valence orbitals is relatively small.

In Table II, we show the energy levels of the final orbitals for ^{20}Ne and ^{24}Mg and in Figs. 1 and 2, we show two typical neutron wave functions for ^{20}Ne (the proton wave functions are very similar).[25] The upper (G) and lower (F) components of the wave functions are labeled by the (nlj) values of the corresponding spherical states. As expected, the mixing is important for levels whose energies are close to the energy surface, while deeply bound levels are almost pure spherical orbitals. As a numerical check on the solution procedure, we have explicitly verified that the two $\frac{1}{2}^-$ orbitals are orthogonal. This is essential,

TABLE II. The final energy eigenvalues of the bound levels in ^{20}Ne and ^{24}Mg.

^{20}Ne		^{24}Mg	
Level	Energy	Level	Energy
	Protons		
$\frac{1}{2}^+$	−40.61	$\frac{1}{2}^+$	−44.60
$\frac{1}{2}^-$	−23.90	$\frac{1}{2}^-$	−29.78
$\frac{3}{2}^-$	−18.31	$\frac{3}{2}^-$	−21.54
$\frac{1}{2}^-$	−11.07	$\frac{1}{2}^-$	−14.35
$\frac{1}{2}^+$	−7.81	$\frac{1}{2}^+$	−11.66
		$\frac{3}{2}^+$	−8.24
	Neutrons		
$\frac{1}{2}^+$	−45.58	$\frac{1}{2}^+$	−50.38
$\frac{1}{2}^-$	−28.56	$\frac{1}{2}^-$	−35.26
$\frac{3}{2}^-$	−22.92	$\frac{3}{2}^-$	−26.94
$\frac{1}{2}^-$	−15.59	$\frac{1}{2}^-$	−19.69
$\frac{1}{2}^+$	−12.08	$\frac{1}{2}^+$	−16.79
		$\frac{3}{2}^+$	−13.28

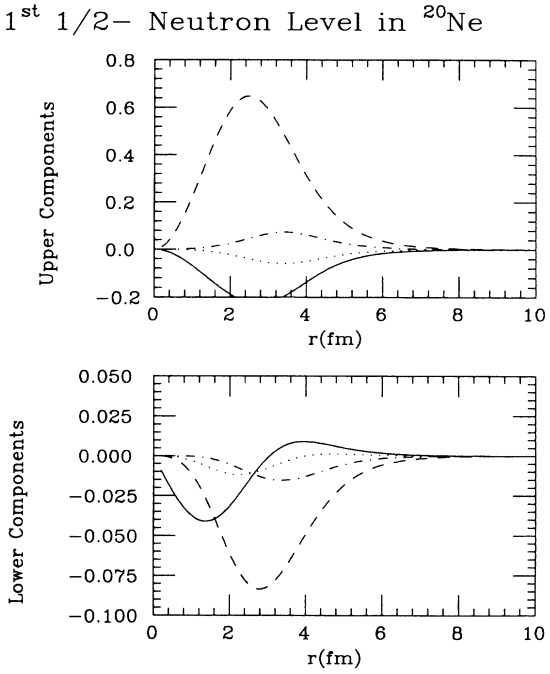

FIG. 1. The first $\frac{1}{2}^-$ neutron level in ^{20}Ne including the $(p\frac{1}{2})$ (solid lines), $(p\frac{3}{2})$ (dashed lines), $f(\frac{5}{2})$ (dotted lines), and $(f\frac{7}{2})$ (dotted-dashed lines) components. The upper components are in the top panel and the lower components are in the bottom panel.

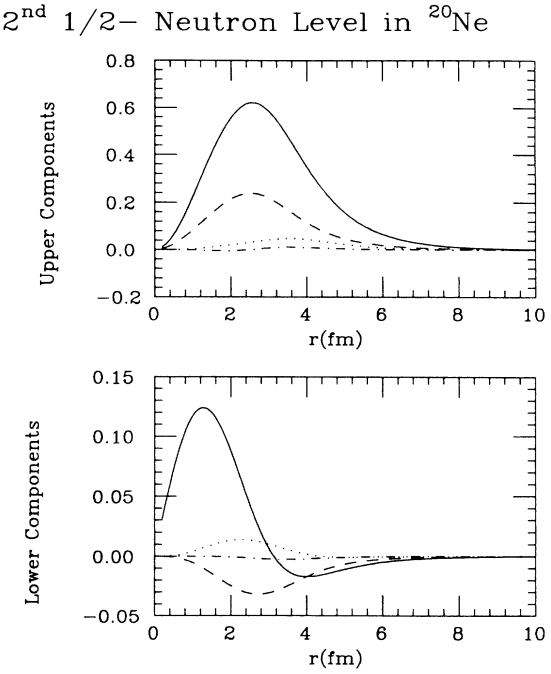

FIG. 2. The second $\frac{1}{2}^-$ neutron level in ^{20}Ne including the $(p\frac{1}{2})$ (solid lines), $(p\frac{3}{2})$ (dashed lines), $(f\frac{5}{2})$ (dotted lines) components, and $(f\frac{7}{2})$ (dotted-dashed lines) components.

since the final orbitals should form an orthonormal set. Figures 3 and 4 show the final baryon density in ^{20}Ne. As is seen in spherical nuclei[7] (relativistically), the central region is slightly depleted with the maximum densities occurring at a distance of roughly 1.5 fm. Although it is difficult to see from these figures, the shape of the surfaces of equal density is a function of the density, with the greatest deformations occurring at intermediate densities (the surface region) and the smallest deformations at high (interior) and low (outside the surface) densities. In general, the shapes of the meson fields are very similar to the shape of the densities. Unfortunately, it is difficult to see any significant difference in the overall shapes of the scalar and vector fields, so it is not possible to draw strong conclusions about the possibility that these fields are driving the deformation. In order to answer the question of how these fields effect the deformation it would be necessary to examine their shapes for deformations other than the equilibrium deformation. Since it is not possible to determine these shapes in a consistent manner, it would be necessary to develop a scheme to shift the meson fields slightly away from equilibrium and observe the reaction of the nucleon densities. As yet, this has not been carried out, but because of its importance to understanding the physics which drives the deformation, it will be the object of future efforts.

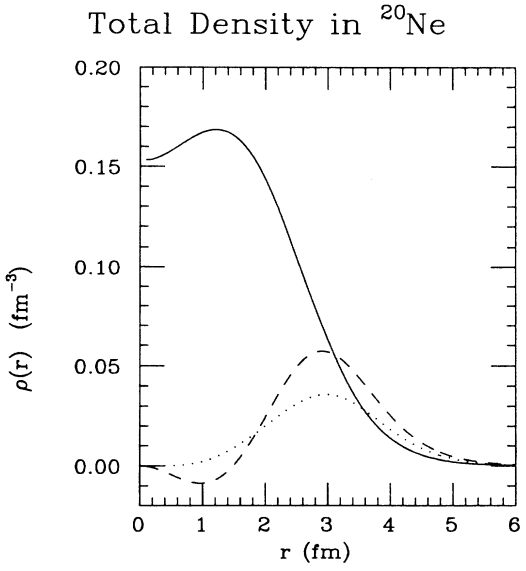

FIG. 3. The baryon density in ^{20}Ne. The solid curve is the $L=0$ component, the dashed curve is the $L=2$ component, and the dotted curve is the $L=4$ component.

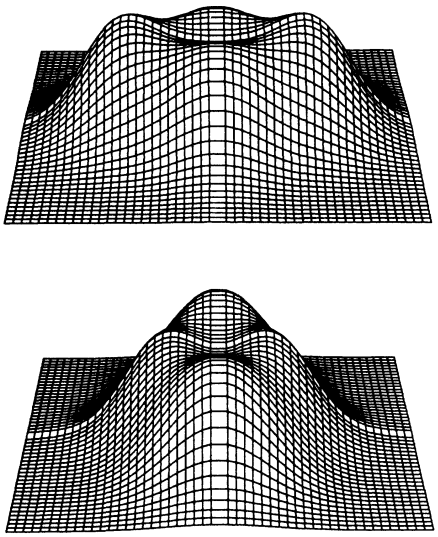

FIG. 4. The baryon density in ^{20}Ne shown as two three dimensional views. The top view is along the symmetry axis and the bottom view is perpendicular to the symmetry axis.

In order to make qualitative comparisons to nonrelativistic calculations we must cast our results in a different form. In the work of Bassichis *et al.*,[13] and Pal and Stamp[14] the deformed orbitals were expanded in a harmonic oscillator basis,

$$|\lambda\rangle = \sum_{nlj} C^{\lambda}_{nlj} |nljm\rangle \ , \tag{23}$$

where the admixture coefficients, C^{λ}_{nlj}, are sufficient to describe the state. Therefore we have calculated the following coefficients from our relativistic orbitals,

$$|C^{\lambda}_{\kappa}|^2 = \int dr [\,|G_{\lambda\kappa}(r)|^2 + |F_{\lambda\kappa}(r)|^2] \tag{24}$$

which should be comparable to the C coefficients in Eq. (23). Both sets of coefficients are normalized to unity:

$$\sum_{nlj} |C^{\lambda}_{nlj}|^2 = \sum_{\kappa} |C^{\lambda}_{k}|^2 = 1 \ . \tag{25}$$

The comparisons for ^{20}Ne are shown in Table III. Similar results (not shown) are obtained for ^{24}Mg. Clearly, the relativistic orbitals are in approximate agreement with the nonrelativistic work, and the discrepancy between the two nonrelativistic calculations is at least as large as the difference between the relativistic and nonrelativistic calculations. A more direct comparison could be made by

TABLE III. A comparison, for ^{20}Ne, of the admixture coefficients (described in the text) found in this work to two previous nonrelativistic calculations. There are some obvious differences that are simply due to the different basis sizes used in the various calculations, but in general, the three calculations are in qualitative agreement.

		Levels				
nlj	Source	$\frac{1}{2}^+$	$\frac{1}{2}^-$	$\frac{3}{2}^-$	$\frac{1}{2}^-$	$\frac{1}{2}^+$
$1s\frac{1}{2}$	This work	0.994				
	Ref. 13	0.995				−0.025
	Ref. 14	0.989				0.007
$1p\frac{1}{2}$	This work		−0.340		0.936	
	Ref. 13		−0.308		0.944	
	Ref. 14		−0.392		0.920	
$1p\frac{3}{2}$	This work		0.932	0.996	0.344	
	Ref. 13		0.939	0.992	0.315	
	Ref. 14		0.920	1.00	0.392	
$1d\frac{3}{2}$	This work	−0.079				−0.249
	Ref. 13	−0.046				−0.310
	Ref. 14	−0.042				−0.393
$2s\frac{1}{2}$	This work					−0.049
	Ref. 13	−0.077				−0.401
	Ref. 14	0.132				−0.457
$1d\frac{5}{2}$	This work	0.077				0.869
	Ref. 13	0.040				0.861
	Ref. 14	0.046				0.798
$1f\frac{5}{2}$	This work		−0.082	−0.053	0.073	
	Ref. 13		−0.094	−0.026	0.070	
	Ref. 14					
$1f\frac{7}{2}$	This work		0.102	0.069		
	Ref. 13		0.110	0.032	−0.026	
	Ref. 14					

expanding the relativistic wave functions in an oscillator basis, but the outcome should be qualitatively the same.

To this point we have discussed only intrinsic state properties. Now, it is useful to develop some approximations for extracting certain ground state properties from the Hartree intrinsic state. First, since the intrinsic state is a superposition of states with various total angular momenta, it is possible to generate the entire ground state rotational band through angular momentum projection. Therefore, the binding energy of the ground state is not equal to the binding energy of the intrinsic state. However, the binding energy of the ground state may be obtained approximately by recognizing that the ground state band should have

$$E_J = E_{\text{g.s.}} + \frac{\hbar^2}{2I} J(J+1) , \tag{26}$$

where I is the nuclear momenta of inertia which may be obtained from the experimental spreading of the levels in the ground state rotational band. (This assumes that the band identified from the experimental energy levels is in fact due to rotational states.) Since the intrinsic ground state has nonzero expectation value of J^2, the energy of the corresponding $J=0$ ground state is

$$E_J = 0 = E_H - \frac{\hbar^2}{2I} \langle J^2 \rangle , \tag{27}$$

where E_H is the Hartree energy of the intrinsic state. This is the same procedure used in the early nonrelativistic work presented in Ref. 13.

Secondly, the rms charge radius may be obtained approximately, by folding the spherical component of the proton density over the proton form factor:[7]

$$\rho_p(r) = \mu^3 e^{-\mu r/8\pi} , \tag{28}$$

where $\mu = 843$ MeV, using

$$\rho_{\text{ch}}(r) = \int dr' \rho(r-r') \rho_p(r') . \tag{29}$$

In addition, anomalous moment corrections may be added as discussed in Ref. 26 by including contributions to the charge density arising from the anomalous moments of the protons and neutrons folded with the appropriate form factors. We also calculate the intrinsic quadrupole moment;

$$Q = \sqrt{16\pi/5} \langle r^2 Y_2^0(\Omega) \rangle \tag{30}$$

and the corresponding deformation parameter

$$\beta = \frac{Q}{1.26 Z \langle r^2 \rangle} . \tag{31}$$

Table IV shows the results for these quantities as well as comparisons to nonrelativistic calculations and experiment. The relativistic quadrupole moments and deformation parameters are somewhat smaller than those found in the nonrelativistic calculations. This indicates that, in general, the relativistic calculation finds smaller overall deformations. This is probably due to the fact that QHD overestimates the nuclear compressibility by almost a factor of 2 which should make the nucleus more resistant to deformations. Since the compressibility is directly related to the surface energy, a high compressibility implies a stiff

TABLE IV. Binding energies, quadrupole moments, deformation parameters and rms radii for various nuclei.

Nuclei	Source	E_H (MeV)	$\hbar^2/2I$ (MeV)	$\langle J^2 \rangle$	$E^{J=0}$ (MeV)	$\langle r^2 \rangle^{1/2}$ (fm)	Q (mb)	β
^{16}O	This work	−78.2	0	0	−78.2	2.75	0	0
	Ref. 13	−47.0	0	0	−47.0		0	0
	Ref. 14	−108.4			−108.4	2.60	0	0
	Experiment				−127.6	2.73	0	
^{20}Ne	This work	−99.5	0.23	16.5	−103.3	2.97	403	0.36
	Ref. 13	−51.8	0.23	18.57	−56.0		524	
	Ref. 14	−132.0			−132.0	2.75	391	0.41
	Experiment				−160.0	3.02	580	
^{24}Mg	This work	−133.2	0.21	16.2	−136.6	3.07	510	0.36
	Ref. 13	−64.7	0.21	17.1	−68.3		640	
	Ref. 14	−162.4			−162.4	2.85	486	0.47
	Experiment				−167.2	3.01	690	
^{40}Ca	This work	−252.0	0	0	−252.0	3.48	0	0
	Ref. 13	−154.7	0	0	−154.7		0	0
	Ref. 14	−228.2		0	−228.4		0	0
	Experiment				−342.1	3.48	0	0
^{42}Ca	This work	−268.3	0.16	15.2	−270.7	3.47	94.9	0.031
	Experiment				−361.9			
^{44}Ca	This work	−285.9	0.13	13.2	−287.6	3.46	170.3	0.056
	Experiment				−381.0			
^{48}Ca	This work	−321.6	0	0	−321.6	3.44	0	0
	Experiment				−416.0	3.47		

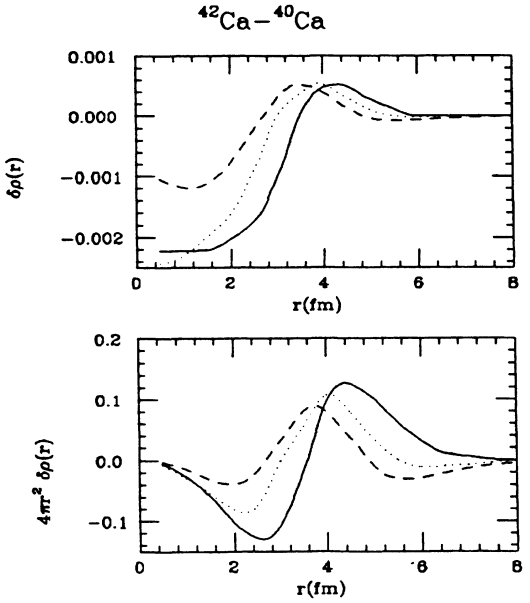

FIG. 5. Charge density difference for $^{42}Ca-^{40}Ca$. The upper panel shows $\delta\rho_{ch}(r)$ and the lower panel shows $4\pi r^2\delta\rho_{ch}(r)$. The solid line represents the experimental results (Ref. 27), the dashed line shows the results of this work and the dotted lines represent the nonrelativistic calculations of Ref. 28.

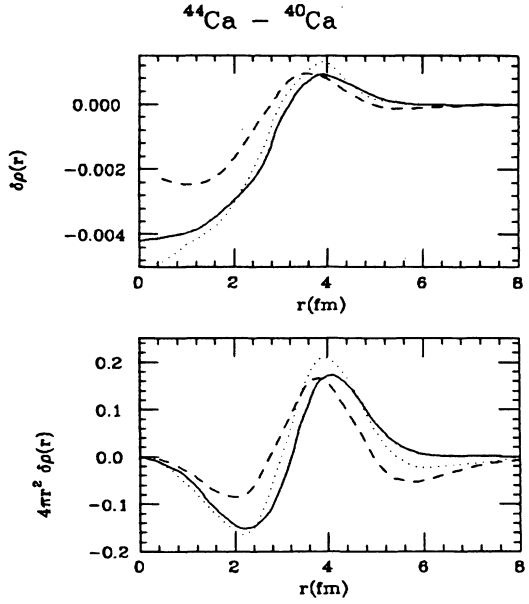

FIG. 6. Charge density difference for $^{44}Ca-^{40}Ca$.

surface which will have a large contribution to the total energy of the deformed system. One should also notice that the rms charge radii (after correction for the anomalous moments) deviate slightly from the experiment. This may be caused by not including the anomalous moment corrections self consistently, since they are not included in the Hartree equations for the fields and orbitals; or by using the same form factor to fold all of the densities. Overall, the agreement of this calculation with previous work and with experiment is quite reasonable.

As a final application of this method, we consider the charge density distributions of the calcium isotopes. In Figs. 5–7 we show the calculated charge density differences for $^{42}Ca-^{40}Ca$, $^{44}Ca-^{40}Ca$, and $^{48}Ca-^{44}Ca$. These figures include the experimental results of Frosch *et al.*,[27] and the nonrelativistic calculations of Brown *et al.*,[28] for comparison. In general, the present calculations are in rough agreement with experiment, however, the qualitative differences suggest that the calculations for the open shell isotopes concentrate too much charge in the central region of the nucleus. This result may also be connected to the compressibility. The calculations presented in these figures do not contain a correction for the anomalous moment and assume that the neutron charge form factor is identically zero. In general, it is reasonable to assume that these effects will be small; however, since inclusion of the anomalous moment corrections will have some effect on the charge distribution (particularly if $N\neq Z$) this approximation may have some effect on the results.

V. SUMMARY AND CONCLUSIONS

In this work, we have developed a self-consistent, relativistic theory of deformed nuclei based on quantum hydrodynamics and the finite Hartree approximation, and have applied this theory to the calculation of deformed orbitals in various light nuclei. Our calculations extend the work of Serot and Horowitz[7] and provide relativistic shell model orbitals for even-even nuclei which may be used as input to a variety of calculations in nuclear structure and reactions. In general, the results of this calculation are in qualitative agreement[29] with experiment and with earlier nonrelativistic calculations. The crucial point of this calculation is that the equilibrium deformation as well as the meson fields and orbitals are determined self-consistently. No additional parameters or adjustments (other than the standard requirements of angular momentum projection) are required to obtain the correct qualitative behavior for the ground states of the nuclei considered. Furthermore, since there is no freedom in this model to enforce a specific deformation, this calculation provides an excellent framework for a detailed investigation of the source of deformations in closed subshell nuclei. Such a deformation could arise from additional terms (possibly tensor couplings) not included in the basic Lagrangian, or from the proper inclusion of the Fock (exchange) terms.

The results of the present calculation indicates that the equilibrium deformations are somewhat smaller than those obtained from previous nonrelativistic calculations and experiment. If this is due to the large compressibility in the mean field model as we believe, it can be easily investigated. By including nonlinear couplings for the scalar field, the compressibility can be lowered and the rela-

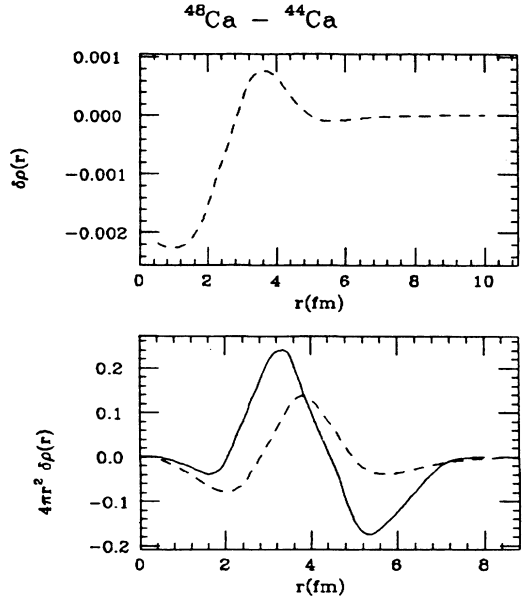

FIG. 7. Charge density difference for ^{48}Ca−^{44}Ca.

tionship between the compressibility and the equilibrium deformation can be determined. This calculation is currently in progress.

As a final note, we mention a few open problems in the area of relativistic deformed nuclear structure that can be addressed using this work as a starting point. First, this model may be extended to odd-mass nuclei by relaxing the restriction of azimuthal and reflection symmetry placed on the equilibrium deformation. This will require that more components of the meson fields be included, but, in principle, the additional field equations may be solved with the methods which are described in this paper. Second, for this parameter set ^{12}C and other closed subshell nuclei are found to be spherically symmetric, even though for many of these nuclei there is experimental evidence that there is a significant deformation in the ground state. This behavior is also seen in many nonrelativistic calculations that also find lower energy ground states for these nuclei by adding a quadrupole term to the Hamiltonian to enforce a nonzero deformation. Such a procedure would be difficult to include self-consistently in the relativistic model; however, it is possible that there are additional, small interactions not included in the starting Lagrangian (tensor terms for example) that could lead to deformations for these nuclei without having a large effect on closed-shell nuclei. This possibility may be easily investigated in the current framework. Finally, there are numerous applications for the orbitals and mean fields that are the results of this work. Some examples are: calculation of electron scattering form factors for deformed nuclei, calculation of transition rates among the members of the rotational band that may be extracted from the intrinsic state, calculations of the effects of a lambda particle impurity (hypernuclei) on the equilibrium deformation, and calculation of vibrational states or fission by allowing for an explicit time dependence. We are currently pursuing various extensions to this calculation, including the application of this technique to heavy nuclei ($A \sim 190$).

Note added in proof. Other parameter sets have been found that yield a deformed ground state for closed subshell nuclei, C. E. Price, R. J. Furnstahl, and G. E. Walker, Bull. Am. Phys. Soc. **32**, 1031 (1987) and to be submitted for publication.

ACKNOWLEDGMENTS

We wish to thank R. J. Furnstahl and B. D. Serot for helpful discussions. This work was supported in part by the National Science Foundation.

APPENDIX: SOLUTION METHODS FOR DEFORMED NUCLEI

The Hartree equations described in Ref. 7 are limited to spherical systems, or doubly closed shell nuclei. These equations and the corresponding solution methods may be extended to nonspherical systems. For the purposes of this work, we have considered only azimuthally symmetric deformations that conserve parity. This is the type of deformation most often adopted nonrelativistically to describe non-closed-shell, even-even nuclei.

The procedure for the numerical solution of Eqs. (13)–(19) is outlined below. First, make an initial guess for the scalar and baryon densities (including a deformation) and the single particle energies. Second, solve the integral form of the boson equations by integrating the densities over the static Greens functions

$$D(r,\theta,r',\theta';m_i) = -m_i \sum_{l \text{ even}} (2l+1) j_l(im_i r_<) \times h_l^{(1)}(im_i r_>) P_l(\theta) P_l(\theta') \quad \text{(A1)}$$

for the mesons and

$$D(r,\theta,r',\theta') = \sum_{l \text{ even}} \frac{r_<^l}{r_>^{l+1}} P_l(\theta) P_l(\theta') \quad \text{(A2)}$$

for the proton. The angular integrations can be performed trivially due to the simple angular dependence and the remaining radial integrals for each term of the boson expansions can be performed using Simpson's rule or other standard techniques. Third, the boson mean fields are substituted into the Dirac equations for the orbitals which are then solved in differential form using a fourth order Runge-Kutta scheme. This procedure is complicated by the coupling between the various components of the orbitals. The difficulty arises because the exact solutions of these equations at large and small r contain one unknown constant for each value of κ included in the summation in Eq. (12). This means that the starting value for the Runge-Kutta scheme contains a prohibitively large number of unknowns. For this reason, the coupled equations are solved iteratively as follows. The equations for the 'dominant' κ (this is the κ that would have been correct for a spherical system) are solved assuming that all of the other components are zero. This is done by using the exact solutions at large and small r to obtain two starting points (with one unknown parameter each) for the Runge-Kutta scheme. Then, the equations are integrated into some matching radius[30] and the unknowns are adjusted so that the upper components are continuous and

the solution is normalized. Then the energy eigenvalue is adjusted using

$$\Delta\epsilon = -[G_\kappa^>(r_{\rm match})F_\kappa^>(r_{\rm match}) - G_\kappa^<(r_{\rm match})F_\kappa^<(r_{\rm match})] \tag{A3}$$

and this procedure is iterated until the eigenvalue converges. Then, the other components are added in sequence and are assumed to have the form

$$\begin{aligned} G_\kappa(r) &= G_\kappa^{\rm general} + G_\kappa^{\rm particular} , \\ F_\kappa(r) &= F_\kappa^{\rm general} + F_\kappa^{\rm particular} . \end{aligned} \tag{A4}$$

After each addition, the general solution is obtained from the Dirac equations [Eqs. (17) and (18)] with no coupling to other components (i.e., $\kappa' = \kappa$ only) using the eigenvalue found above. The exact solutions at large and small r are used to provide starting values for the Runge-Kutta routine and again each contains one unknown parameter. The general solution found in this manner is not continuous at the matching radius. The particular solution is found from Eqs. (17) and (18) including the coupling to the other components by assuming that, for the particular solution, the unknown constants in the exact solutions at large and small r are zero. This solution is also not continuous at the matching radius. The two unknowns in the general solution are adjusted so that the complete solutions (general plus particular) for both $G_\kappa(r)$ and $F_\kappa(r)$ are continuous. When all necessary components have been included,[31] the solution for the dominant κ is reevaluated including the coupling to the other components as a particular solution. One unknown constant in the general solution is determined by insisting that $G_\kappa(r)$ be continuous at the matching radius and the other is taken from the previous iteration. Then, after normalization

$$\int_0^\infty dr \sum_\kappa [\,|G_\kappa(r)|^2 + |F_\kappa(r)|^2] = 1 \tag{A5}$$

the eigenvalue is adjusted using Eq. (A3) and the solution for this κ is repeated until the eigenvalue has converged to within a given tolerance. Then in the last iteration both unknowns may be adjusted by insisting that both G and F be continuous at the matching radius. This procedure is then iterated from the second step outlined above, and when the eigenvalue has converged to within a smaller tolerance (0.1 times the tolerance above is sufficient) the complete solution for the given orbital has been obtained and contains up to $2L_{\rm max}+1$ consistently determined components.[31] Finally, the orbitals are used to determine a new guess for the densities and the entire procedure is iterated until all of the energy eigenvalues (and hence the meson fields) have converged.

In addition to the routine tests involving the mesh size in the Runge-Kutta routine and the tolerances used to determine convergence, spherical nuclei, like ^{16}O and ^{40}Ca, provide a strong test of the computer code. By making an initial guess for the densities which includes a substantial deformation, the code may be tested by a direct comparison to the results of Horowitz and Serot.[7] We find that our results are in complete agreement with their calculations, and that the inclusion of the initial deformation has very little effect on the rate of convergence of the solution.

*Permanent address: Physics Division, Argonne National Laboratory, Argonne, IL 60439.

[1]J. R. Shepard, E. Rost, E. R. Siciliano, and J. A. McNeil, Phys. Rev. C **29**, 2243 (1984).
[2]R. J. Furnstahl, Phys. Lett. **152B**, 313 (1985).
[3]L. G. Arnold, B. C. Clark, R. L. Mercer, and P. Schwandt, Phys. Rev. C **23**, 1949 (1981), and references cited therein.
[4]J. D. Walecka, Ann. Phys. **83**, 491 (1974).
[5]B. C. Clark, R. L. Mercer, and P. Schwandt, Phys. Lett. **122B**, 211 (1983).
[6]B. D. Serot and J. D. Walecka, Adv. Nucl. Phys. **16**, 1 (1986), and references cited therein.
[7]C. J. Horowitz and B. D. Serot, Nucl. Phys. **A368**, 503 (1981).
[8]B. D. Serot, Phys. Lett. **107B**, 263 (1981).
[9]R. J. Furnstahl and B. D. Serot, Indiana University Nuclear Theory Center, Report No. 86-3, 1986.
[10]M. W. Price, in Proceedings of the Los Alamos Workshop on Relativistic Dynamics and Quark Nuclear Physics (in press).
[11]M. W. Price, Ph.D. thesis, Indiana University, 1986 (unpublished); M. W. Price and G. E. Walker (unpublished).
[12]C. E. Price and G. E. Walker, Phys. Lett. **155B**, 17 (1985).
[13]W. H. Bassichis, A. K. Kerman, and J. P. Svenne, Phys. Rev. **160**, 746 (1967).
[14]M. K. Pal and A. P. Stamp, Phys. Rev. **158**, 924 (1967).
[15]K. W. Schmid, E. Hammaren, and F. Grummer, in *Nuclear Structure at High Spin Excitation, and Momentum Transfer,* edited by Herman Nann (AIP, New York, 1985).
[16]I. Talmi, in *Interacting Bosons in Nuclear Physics,* edited by F. Iachello (Plenum, New York, 1978).
[17]Primarily, we have adopted the conventions of Bjorken and Drell (Ref. 18) for four-vector notation and the Dirac equation, and those of Brink and Satchler (Ref. 19) for angular momentum. All equations are presented in physical units, $\hbar = c = 1$.
[18]J. D. Bjorken and S. D. Drell, *Relativistic Quantum Mechanics* (McGraw-Hill, New York, 1964).
[19]D. M. Brink and G. R. Satchler, *Angular Momentum* (Clarendon, Oxford, 1968).
[20]M. E. Rose, *Relativistic Electron Theory* (Wiley, New York, 1961).
[21]D. J. Rowe, *Nuclear Collective Motion* (Methuen and Co. Ltd., London, 1970).
[22]G. Ripka, Adv. Nucl. Phys. **1**, 183 (1968).
[23]R. E. Peierls and J. Yoccoz, Proc. Phys. Soc. (London), Sect. A **70**, 381 (1957).
[24]S. G. Nilsson, Mat. Fys. Medd. Dan. Vid. Selsk **29**, No. 16 (1955).
[25]These orbitals and the Fortran code which generates them are available from the authors.
[26]L. D. Miller, Phys. Rev. C **14**, 706 (1976).
[27]R. F. Frosch *et al.*, Phys. Rev. **174**, 1380 (1968).
[28]B. A. Brown, S. E. Massen, and P. E. Hodgson, J. Phys. G **5**,

1655 (1979).

[29]After this work was completed and submitted for publication, a similar investigation by Lee *et al.* appeared [S. J. Lee *et al.*, Phys. Rev. Lett. **57**, 2916 (1986)]. Our results are in disagreement with their conclusions. They find that the relativistic theory gives unsatisfactory results for precisely the same deformed nuclei which we study. In fact Lee *et al.* adopt input parameters that do not give satisfactory fits for spherical nuclei [and are not those obtained in studies of spherical nuclei, see Refs. 6 and 7 and B. D. Serot (private communication)]. As an example, in Table I of Lee *et al.*, a value of 3.12 fm is quoted as their result for the rms charge radius of *spherical* ^{40}Ca. Standard input parameters yield a rms charge radius of 3.48 fm which is also the experimental result (see Table IV herein). The computational methods utilized are also quite different. (*Note added in proof.* Our conclusions are consistent with those of W. Pannert, P. Ring, and J. Boguta, submitted to Phys. Rev. Lett.)

[30]The matching radius should be chosen in the exponential tail of the solution away from all nodes.

[31]If $L_{\max}$ is the highest l value in the boson expansions and $\kappa_{\rm sph}$ is the dominant κ value in the nucleon expansion, then the sum over κ in the nucleon expansion is allowed to run from $|\kappa_{\rm sph}-L_{\max}|$ to $\kappa_{\rm sph}+L_{\max}$. For the results shown in this paper, the boson expansion has been truncated at $L_{\max}=4$. We have used $L_{\max}=6$ in several calculations (in ^{20}Ne as an example) to test the convergence of the results as a function of l and have found for the light nuclei cases tested that the $l=6$ contribution is very small. For example, the total binding energy in ^{20}Ne is lowered by less than one percent by the inclusion of the $l=6$ term.